Multifractal modeling of anomalous scaling laws in rainfall

R. Deidda[1], R. Benzi[2], and F. Siccardi[3]

[1]CRS4, Centro di Ricerca, Sviluppo e Studi Superiori in Sardegna.
Cagliari, Italy
[2]Dipartimento di Fisica, Università "Tor Vergata", Via della Ricerca
Scientifica, I-00133 Roma, Italy
[3]Istituto di Idraulica, Facoltà di Ingegneria, Università di Genova,
Via Montallegro 1, I-16145 Genova, Italy

Manuscript submitted to

Water Resources Research

Manuscript version from May 11, 1998

Offset requests to:
Roberto Deidda
CRS4
Via Nazario Sauro, 10
Cagliari, I-09123 Italy.

Send proofs to:
Roberto Deidda
CRS4
Via Nazario Sauro, 10
Cagliari, I-09123 Italy.

Abstract

The coupling of hydrological distributed models to numerical weather predictions outputs is an important issue for hydrological applications such as forecasting of flood events. Downscaling meteorological predictions to the hydrological scales requires the resolution of two fundamental issues regarding precipitation, namely: 1) understanding the statistical properties and scaling laws of rainfall fields; 2) validation of downscaling models that are able to preserve statistical characteristics observed in real precipitation. In this paper we discuss the first issue by introducing a new multifractal model that appears particularly suitable for random generation of synthetic rainfall. We argue that the results presented in this paper may be also useful for the solution of the second question. Statistical behavior of rainfall in time is investigated through a high resolution time series recorded in Genova (Italy). The multifractal analysis shows the presence of a temporal threshold, localized around $10 \div 20$ hours, which separates two ranges of anomalous scaling laws. Synthetic time series, characterized by very similar scaling laws to the observed one, are generated with the multifractal model. The potential of the model for extreme rainfall event distributions is also discussed. The multifractal analysis of GATE radar fields have shown that statistical properties of rainfall in space depend on time durations over which precipitation is accumulated. Further analysis of some rainfall fields produced with a meteorological limited area model exhibited the same anomalous scaling as the GATE fields.

Correspondence to: Roberto Deidda

1

1 Introduction

In the last 30 years much research and many contributions have been focused both on statistical analysis of extreme events distributions and on stochastic modeling of rainfall in time and space. Current atmospheric numerical modeling makes operational rainfall field prediction feasible with significant short-range reliability. The problem of "downscaling" of the precipitation fields is now very topical as it represents a natural link between the scales of meteorological applications and those of surface hydrologic modeling. Meteorological centers for numerical weather prediction distribute forecasts of precipitation fields with grid-size spatial resolutions ranging from 10^4 km^2 (general circulation models, GCMs) to 10^2 km^2 (limited area models, LAMs). For hydrological applications we need, instead, to have precipitation predictions at the smaller spatial and temporal scales of basins. Thus, given average precipitation depths at large scale, e.g., those from meteorological models, accurate downscaling to enable simulation of precipitation fields over smaller scales, preserving correctly the statistical properties observed on real signals across the different scales, would be very useful.

Past research on space-time stochastic modeling of precipitation has addressed mainly two classes of models: cluster-based and fractal/multifractal models. A common assumption of cluster-based models is that the rainfall process be organized in a preferred hierarchy of scales in space and time. This hierarchy of scales would represent, with more or less detail, the process of rainband arrival, the cluster organization of cells within a rainband, and the life-cycle of cells belonging to each cluster. LeCam [1961] can be considered the precursor of cluster-based models, while the most popular implementation of such models is represented by the WGR model [Waymire et al., 1984]. Following the second line of research, more recent papers deal with multifractal models based on random cascades [Gupta and Waymire, 1993; Hubert et al., 1993; Kumar and Foufoula-Georgiou, 1993; Ladoy et al., 1993; Lovejoy and Schertzer, 1992; Schertzer and Lovejoy, 1987; Tissier et al., 1993]. Many of the multifractal models proposed for simulation of synthetic precipitation fields were first applied to simulate anomalous scaling of velocity fields in turbulent flows

[Benzi et al., 1984].

At the moment the multifractal theory represents the most powerful approach to nonlinear phenomena such as turbulent velocity fluctuation or intermittency of precipitation. The multifractal formalism allows a robust statistical control over any moment of a given distribution of measures, if some kind of similarity holds over a range of scales. Analysis and comparison between real signals and simulated ones must address the behavior of high moment distributions over different scales of interest, rather than, for example, the fractional coverage of wetted areas or rain duration. Two reasons for this are: 1) fractional coverage can be biased by the discrete sampling of data, especially for smaller scales, and, more importantly, 2) the strongest events can be correctly captured only if we are able to reproduce higher order moments.

From the analysis of statistical properties of rainfall in time or in space, such as presented in this paper, it is clear that precipitation is a strongly intermittent and nonlinear process: multifractal analysis shows indeed that rainfall fields are characterized, both in space and in time, by anomalous scaling laws, whose scaling exponents can be expressed as convex, and so nonlinear, functions of the moments. This means that simple fractal models like the β-model proposed 20 years ago by Frish et al. [1978] for turbulence intermittency, and recently by Over and Gupta [1994] for generation of rainfall, are not the best way to create synthetic fields of precipitation, because scaling exponents of fractal models depend linearly on the moments.

In this paper we review briefly the multifractal theory and a new general concept of scaling [Benzi et al., 1996], and we point out the important role that infinitively divisible distributions (i.d.d.), such as log-Poisson, have on multiplicative processes. We then present the main features of a recently developed multifractal model [Deidda, 1997], that can be applied to rainfall downscaling problems. The model recalls some ideas from Benzi et al. [1993a], but it is based on an expansion of positive definite wavelets with coefficients belonging to a stochastic cascade. In such a way, we are able to construct positive definite multifractal measures in spaces of any dimension. The analytical derivation of the theoretical anomalous scaling laws of the

3

generated signal is also presented. In view of possible application of this model for generating synthetic rainfall, we discuss some examples of simulations in one and two-dimensional spaces that illustate the good agreement between the theoretically expected scaling laws and those obtained from Monte Carlo simulations.

Results of multifractal analysis of a high resolution (1 minute) time series of precipitation recorded in Genova over 8 years have shown the existence of two ranges of anomalous scaling for time smaller and longer than a duration threshold. The physical meaning and explanation of the threshold is addressed later in the paper. However, within each range, the analysis of moments of signals displays a nonlinear behavior that justifies the multifractal approach. In order to test the ability of the model to generate time series of precipitation we have compared scaling laws of synthetic time series with those of the observed one. Additional verification of model performance was conducted on rainfall yearly maxima at different time duration: extreme event distributions of synthetic signals were successful compared with those of the observed time series. The positive results of this comparison enables us, when no measure is available at small scales, to use models for stochastic downscaling of precipitation to transfer information from time series at larger scales.

We also discuss in this paper the analysis of statistical properties of precipitation in space. Results on spatial fields of rainfall are based on radar observations during the GARP (Global Atmospheric Research Program) Atlantic Tropical Experiment, often referred as the GATE experiment, and on some precipitation fields obtained by a numerical simulation at very high resolution (10 km) performed with a LAM. We show that the anomalous scaling laws of rainfall in space depend strongly on the time scale over which precipitation is accumulated. To demonstrate this we have analyzed the GATE fields not only at their original resolution of 15 minutes, but also the fields accumulated over 30 minutes, 1 hour and up to 24 hours. As expected, rainfall is characterized by a stronger intermittency for shorter accumulation times. The LAM precipitation fields also show anomalous scaling in the range from 10 to 160 km, but the most interesting result is that the statistical properties of the LAM precipitation, stored every 6 hours of simulation, are very close to that found for GATE at the corresponding 6-hour accumulation time.

This paper is organized as follows: in section 2 a review of recent developments in the scaling theory of three-dimensional turbulent flows is presented and connections with rainfall data analysis are emphasized; a new multifractal model for random generation of synthetic rainfall and theoretical derivation of scaling laws are presented in section 3; statistical behavior of a high resolution time series observed at the University of Genova and some applications of the multifractal model for generation of synthetic rain time series are discussed in section 4; the spatial statistical properties of rainfall fields are investigated through GATE campaign data-sets and from precipitation fields produced by a limited area model simulation in section 5. Finally, a summary and conclusions of this research are drawn in section 6.

2 Scale covariance and generalized scaling

We review recent developments in the multifractal theory of fully developed turbulence. Our aim is to introduce the concepts of generalized scaling and of scale covariance [Benzi et al., 1993b, 1995, 1996], which will be used in the present paper to analyze and simulate the statistical properties of rainfall in time and in space. We will formulate our review directly in the language useful for multifractal analysis of rainfall data.

Let us consider a positive random field $P(x)$ ($P(x) \geq 0$) defined on the set $x \in [0, L]$. Without loss of generality, $P(x)$ is normalized to 1, i.e. $\int_0^L P(x)dx = 1$, for any realization. Our primary interest is to discuss the scaling properties of the quantity:

$$\int_x^{x+r} P(y)dy \equiv \mu_x(r) \tag{1}$$

$P(x)$ is said to display anomalous scaling properties if:

$$< [\mu_x(r)]^q > \sim r^{\zeta(q)} \tag{2}$$

where $\zeta(q)$ is a nonlinear function of q. The scaling exponents $\zeta(q)$ are also referred to as multifractal exponents of $P(x)$. In equation (2) $< \cdots >$ stands for both x-average and ensemble average.

It is useful to introduce another quantity strictly connected to $\mu_x(r)$, namely:

$$\sigma_x(r) = \frac{1}{r}\int_x^{x+r} P(y)dy = \frac{\mu_x(r)}{r} \tag{3}$$

It follows that, if equation (2) holds, one obtains:

$$< [\sigma_x(r)]^q >\sim r^{\zeta(q)-q} \tag{4}$$

Hereafter we shall also use the notation $\tau(q) = \zeta(q) - q$. Because of the normalization $\int_0^L P(x)dx = 1$ we have:

$$\zeta(1) = 1 \quad ; \quad \tau(1) = 0 \tag{5}$$

Note that equations (5) are true independently of the (anomalous) scaling properties of $P(x)$.

A way to give a physical interpretation of (2) and (4) is based on the multifractal formalism. One assumes that $\sigma_x(r) \sim r^\alpha$, in a suitable range of r, with probability $Q_r(\alpha) \sim r^{d-D(\alpha)}$, where $D(\alpha)$ is the fractal dimension, at scale r, where the local scaling condition $\sigma_x(r) \sim r^\alpha$ holds, and d is the dimension of the embedded space (in our case $d = 1$).

It then follows that:

$$< [\sigma_x(r)]^q >\sim \int r^{q\alpha+d-D(\alpha)}d\alpha = r^{\tau(q)} \tag{6}$$

Applying a saddle point estimate of the above integral we obtain $\tau(q) = \inf_\alpha [q\alpha + d - D(\alpha)]$. Let us remark that, in the multifractal formalism, both $\sigma_x(r)$ and $Q_r(\alpha)$ are assumed to exhibit scaling behavior with respect to r.

A simple way to build up a multifractal field $P(x)$ is to use a cascade model based on random multipliers. Let us consider a set of length scales $r_n \equiv 2^{-n}L$ and let us define a *generator* η_i to be:

$$\sigma_x(r_i) \equiv \eta_i\sigma_x(r_{i-1}) \tag{7}$$

Then it follows that:

$$\sigma_x(r_n) = \prod_{i=1}^{n} \eta_i\sigma_x(L) \tag{8}$$

6

Let us also suppose that the set of η_i are identically distributed independent random variables, with $\eta_i \geq 0$. Then we have:

$$< [\sigma_x(r_n)]^q > \equiv \prod_{i=1}^{n} < \eta_i^q > < \sigma_x(L)^q > \tag{9}$$

Because $\sigma_x(L) = 1/L$, we obtain:

$$< [\sigma_x(r_n)]^q > = L^{-q} < \eta^q >^n = L^{\log_2 <\eta^q> - q} r_n^{-\log_2 <\eta^q>} = C(q) r_n^{-\log_2 <\eta^q>} \tag{10}$$

Using (6) and (10) we can identify $\tau(q) = -\log_2 < \eta^q >$. Because $\tau(1) = 0$, we must require $< \eta > = 1$.

The result obtained in (10) relies upon the fact that $n = -\log_2(r_n/L)$ and that all η_i are independently identical distributed. In general one can define $r_n = L\lambda^{-n}$, where $\lambda \geq 2$ is called branching number. Alternatively one can write (8) as a production of $n(r)$ random multipliers η_i, where $n(r) = -\log_\lambda(r/L)$. This tells us that, for a given probability distribution of η_i, the probability distribution of $\sigma_x(r)$ depends on the branching number λ.

Let us now consider three arbitrary scales $r_1 > r_2 > r_3$ and let us define the random multiplier η_{ij} through the relation:

$$\sigma_x(r_i) = \eta_{ij}\sigma_x(r_j) \tag{11}$$

By (11) we have:

$$\eta_{13} = \eta_{12}\eta_{23} \tag{12}$$

Equation (12) is true regardless of the ratios r_1/r_2 and r_2/r_3 are. Let P_{ij} be the probability distribution of η_{ij}. Now we are interested in the probability distribution P_{ij} which is functionally invariant under transformation (12) or the equivalent:

$$\log \eta_{13} = \log \eta_{12} + \log \eta_{23} \tag{13}$$

Thus our search is restricted to probability distributions that are stable under convolution. For independently distributed random variables a solution to this problem can be given in complete form. If the variables are correlated the problem becomes

7

much more difficult to solve, as is well known from the modern theory of second order phase transition. For the time being we shall restrict ourselves to independent random variables. In this case, for instance, the Gaussian and the Poisson distribution are well known examples of probability distributions that are stable under convolution.

Equivalently, a simple solution to this problem is given by all probability distributions P_{ij} such that:

$$< \eta_{ij}^p > = \prod_{k=1}^{M} \left[\frac{g_k(r_j)}{g_k(r_i)} \right]^{\gamma_k(p)} \tag{14}$$

for any function g_k and γ_k. We remark that equation (14) represents the most general solution to the problem, independently of the scale ratio r_i/r_j. Probability distributions satisfying (14) will be referred to as <u>scale covariant</u>.

In order to understand clearly the meaning of (14) we want to give an example based on a random log-Poisson multiplicative process. Namely we assume that:

$$\eta_{ij} = A_{ij} \beta^{y_{ij}} \tag{15}$$

where $\beta < 1$ is a constant parameter, A_{ij} is a scale dependent parameter, and y_{ij} is a Poisson process with scale dependent parameter C_{ij} ($E[y_{ij}] = c_{ij}$):

$$P(y_{ij} = m) = \frac{C_{ij}^m e^{-C_{ij}}}{m!} \tag{16}$$

This example also provides a link between equation (14) and the case of probability distributions that are stable under convolution.

By using (16) we obtain:

$$< \eta_{ij}^p > = A_{ij}^p \exp\left[C_{ij} \left(\beta^p - 1 \right) \right] \tag{17}$$

Assuming $\gamma_1(p) = p$ and $\gamma_2(p) = \beta^p - 1$, equation (17) is equivalent to (14) if we write $A_{ij} = g_1(r_j)/g_1(r_i)$ and $\exp C_{ij} = g_2(r_j)/g_2(r_i)$. Moreover, because of the constraint $< \eta_{ij} > = 1$, we also have $A_{ij} \exp\left[C_{ij} \left(\beta - 1 \right) \right] = 1$, or in terms of g_1 and g_2:

$$\frac{g_1(r_j)}{g_1(r_i)} = \left[\frac{g_2(r_j)}{g_2(r_i)} \right]^{(1-\beta)} \tag{18}$$

Finally we obtain:

$$< \eta_{ij}^p >= \left[\frac{g_2(r_j)}{g_2(r_i)}\right]^{[p(1-\beta)+\beta^p-1]} \tag{19}$$

Equation (19) implies:

$$< [\sigma_x(r)]^p >\sim g_2(r)^{-[p(1-\beta)+\beta^p-1]} \tag{20}$$

which is described by (14) with $M = 1$.

Only if we assume:

$$g_2(r) = r^A \tag{21}$$

can we recover a scaling law for $< \sigma_x(r)^p >$.

This example highlights an important point in our discussion: the scaling of $\sigma_x(r)$ with respect to r is not a necessary consequence of a cascade model based on random multipliers. A scaling law is observed only by assuming that the parameters describing the random multipliers show scaling with respect to r.

In the case of the scale covariance random multiplicative cascade model (hereafter referred as the scale covariance model) we can observe for $M = 1$ a new kind of generalized scaling, hereafter referred to as extended self similarity (ESS). Indeed by (14) and (20) we have $< \sigma_x(r)^p >= g(r)^{-\gamma(p)}$. Therefore, even if $g(r)$ does not show any scaling in r, we have:

$$< \sigma_x(r)^p >=< \sigma_x(r)^q >^{\frac{\gamma(p)}{\gamma(q)}} \tag{22}$$

for any $p \neq q$ and $p \neq 1$, $q \neq 1$. Equation (22) highlights the fact that the field $\sigma_x(r)$ is characterized by anomalous scaling, where the word anomalous refers to dimensional counting.

By using the log-Poisson case as an example, we can provide a physical meaning to the scale covariance model and extended self similarity (22).

Let us first assume that the scaling with respect to r holds as for (21). In this case we have $\tau(p) = A[-p(1-\beta) - \beta^p + 1]$. For $p \to \infty$ the asymptotic form of $\tau(p)$ is:

$$\tau(p) \to -A(1-\beta)p + A \tag{23}$$

9

Using the analog to equation (4), but for d-dimensional spaces, we must write $\zeta(p) = \tau(p) + pd$; so the asymptotic form of the multifractal exponents is $\zeta(p) \rightarrow p[d - A(1 - \beta)] + A$. Following the multifractal interpretation we can define A in terms of the fractal dimension D_∞, defined as the fractal dimension of the set where the strongest events take place:

$$A = d - D_\infty \tag{24}$$

Finally we obtain:

$$\zeta(p) \rightarrow p[D_\infty + \beta(d - D_\infty)] + (d - D_\infty) \tag{25}$$

It is interesting to observe that, by using (24), equation (21) implies that $g_2(r)$ is the probability distribution for the most extreme events. Such a probability distribution shows a scaling behavior only if a geometrical interpretation, in terms of fractal dimension, holds. Generalizing the concept of multifractals, we can think of D_∞ as the fractal dimension of the most intense fluctuation at scale r:

$$D_\infty = d - \frac{\log g_2(r)}{\log r} \tag{26}$$

where now $g_2(r)$ <u>is not</u> scaling in r. In this case, we lose the scaling properties of $\sigma_x(r)$ and we recover the ESS generalized scaling (22).

We make two important remarks in closing this review. The first has to do with the extension of generalized scaling of the quantity $\mu_x(r)$. Using (3) we see that:

$$< \mu_x(r)^p > = r^p < \sigma_x(r)^p > \tag{27}$$

Thus generalized scaling seems not to hold for $\mu_x(r)$. In fact we can define a dimensionless quantity $R_p(r)$ as:

$$R_p(r) = \frac{< \mu_x(r)^p >}{< \mu_x(r)^n >^{\frac{p}{n}}} \tag{28}$$

where $n \geq 2$. By using (28), (27) and (22) we have:

$$R_p(r) = \frac{< \sigma_x(r)^p >}{< \sigma_x(r)^n >^{\frac{p}{n}}} = < \sigma_x(r)^p >^{1 - \frac{p\gamma(n)}{n\gamma(p)}} = R_q(r)^{\left[\frac{\gamma(p) - \frac{p}{n}\gamma(n)}{\gamma(q) - \frac{q}{n}\gamma(n)}\right]} \tag{29}$$

For the log-Poisson example we have for $n = 2$:

$$R_p(r) = R_q(r)^{\left[\frac{(1-\beta^p)-\frac{p}{2}(1-\beta^2)}{(1-\beta^q)-\frac{q}{2}(1-\beta^2)}\right]} \tag{30}$$

Equation (29) holds for any scale covariant model with $M = 1$. Note that the scaling exponent of (30) does not depend on the function $g_2(r)$. Equation (30) can also be considered as a generalized form of extended self similarity (GESS).

The second point concerns the role of the log-Poisson distribution or, more generally, the role of infinitively divisible distributions (i.d.d.). As far as independent random multipliers are used, the choice of an i.d.d. can be done in such a way to satisfy scale covariance. So far, all published models for random multipliers based on i.d.d. can be generalized in the form (14) with $M = 1$. Therefore, for those models, generalized scaling (22) or (29) should hold.

Finally let us also comment about the fact that most emphasis has been addressed on the universal value, if any, of the scaling exponents $\tau(p)$. In light of the discussion in this section we can state that the exponents $\tau(p)$ may not be universal while their ratios $\tau(p)/\tau(q)$ may show universal values. This question will be addressed in the following sections.

3   A model for synthetic rainfall

In this section we develop a simple model to simulate a synthetic, positive definite, rainfall field with predefined anomalous scaling exponents. As we shall see, the model can be adjusted to show any set of anomalous exponents explained by a random multiplicative process. Moreover, it can be easily generalized to include generalized scaling such as ESS (22) or GESS (29). We point out that the comparison between synthetic rainfall fields against observed ones will be extremely useful in order to understand whether observed features of rainfall data, such as extreme events, are correctly reproduced by synthetic fields. In subsection 3.1 we discuss our main theoretical result. In subsection 3.2 we show, using the example of the log-Poisson distribution, how to include the concept of generalized scaling in the

framework of the synthetic field. In subsection 3.3 we discuss some examples of anomalous scaling obtained using numerical simulations.

3.1 Construction of signals and anomalous scaling

Let us consider a positive definite field $\phi(x)$ with $x \in [0,1]$ and let us define the structure functions S_q as:

$$S_q(r) = < \left[\int_\xi^{\xi+r} \phi(x)dx \right]^q >$$

(31)

where $< \cdots >$ is now a spatial average, defined as an integral over all possible starting points ξ: $< f > = c \int f d\xi$. We want to show how to construct the random field $\phi(x)$ showing anomalous scaling in the structure functions S_q, namely

$$S_q(r) \sim r^{\zeta(q)}$$

(32)

where the symbol $\sim$ is used to indicate quantities that differ for a multiplicative constant.

The generation of the signal $\phi(x)$ is based on the following "wavelet" decomposition with coefficients belonging to a dyadic stochastic cascade:

$$\phi(x) = \sum_{j=0}^N \sum_{k=0}^{2^j-1} \alpha_{j,k} \psi_{j,k}(x)$$

(33)

where j is an index for cascade level, varying from 0 (first element) to N (number of cascade levels); k is the position index, varying from 0 to $2^j - 1$ in the j-th cascade level; $\psi_{j,k}(x)$ is the wavelet on k-th position on level j; while $\alpha_{j,k}$ is the coefficient extracted from the stochastic cascade.

The wavelets $\psi_{j,k}(x)$ are normalized in modulus and are obtained by stretching and shifting of the same basis wavelet $\Psi(x)$ that is positive definite and integrable for $x \in [0,1]$ and zero elsewhere:

$$\psi_{j,k}(x) = 2^j \Psi(2^j x - k)$$

(34)

Using this definition it is easy to show that the normalization in modulus of wavelets $\psi_{j,k}(x)$ can be derived from the norm of the basis function $\Psi(x)$:

$$\int_0^1 \psi_{j,k}(x)dx = \int_0^1 \Psi(z)dz = 1$$

(35)

The following Gaussian distribution is an example of a basis wavelet:

$$\Psi(x) = \begin{cases} c \, \exp\left[-\frac{1}{2}\left(\frac{x-\mu}{\sigma}\right)^2\right] & x \in [0,1] \\ 0 & x \notin [0,1] \end{cases} \tag{36}$$

where $\mu = \frac{1}{2}$, $\sigma = 0.15 \div 0.2$ and $c \cong \frac{1}{\sigma\sqrt{2\pi}}$ is a normalization constant. Figure 1 shows the basis function (36), with $\sigma = 0.15$, and wavelets $\psi_{j,k}(x)$ obtained using relation (34) over the first two levels.

The stochastic cascade (Figure 2) is derived by a multiplicative process: each *son* $\alpha_{j,k}$ at the j-th level is obtained multiplying the corresponding *father* at level $j-1$ by an independent and identically distributed random variable η, called the generator:

$$\alpha_{j,k} = \alpha_{j-1,\frac{k}{2}}\eta_{j,k} \tag{37}$$

The moments of the random variable $\alpha_{j,k}$ do not depend on the position index k and can be evaluated by (38), where the bar denotes ensemble average:

$$\overline{\alpha_{j,k}^q} = \overline{\alpha_j^q} = \alpha_0^q \overline{\eta^q}^j \tag{38}$$

The first term α_0 of the random cascade can be obtained by substituting equations (33), (35) and (38) into the integral of the signal $I = \int_0^1 \phi(x)dx$:

$$\alpha_0 = \frac{I}{\sum_{j=0}^{N} 2^j \overline{\eta}^j} \tag{39}$$

The first order structure function S_1 of the signal (33) can be written:

$$S_1(r) = \sum_{j=0}^{N} \sum_{k=0}^{2^j-1} \alpha_{j,k} < \left[\int_\xi^{\xi+r} \psi_{j,k}(x)dx\right] > \sim r^{\zeta(1)} \tag{40}$$

where linear operators $<>$, $\sum$ and integral symbols were exchanged. Introducing an integral function $F(u) = \int_0^u \Psi(x)dx$, we can substitute the integral in square brackets of the previous equation by the following expression:

$$\int_\xi^{\xi+r} \psi_{j,k}(x)dx = 2^j \int_\xi^{\xi+r} \Psi(2^j x - k)dx = F(2^j \xi + 2^j r - k) - F(2^j \xi - k) \tag{41}$$

13

We can now define a distribution $G_1(r) = < F(\xi + r) - F(\xi) >$, that is a function of the scale r, as the variable ξ is saturated from the spatial average $<>$. The G_1 distribution allows us to evaluate the new quantity in square brackets:

$$< \left[F(2^j \xi + 2^j r - k) - F(2^j \xi - k) \right] > = 2^{-j} G_1(2^j r) \tag{42}$$

Finally the first order structure function S_1 can be estimated using the last two equations, together with (38) and (39):

$$S_1(r) = \sum_{j=0}^{N} \sum_{k=0}^{2^j - 1} \alpha_{j,k} 2^{-j} G_1(2^j r) = \sum_{j=0}^{N} 2^j \overline{\alpha_j} 2^{-j} G_1(2^j r) = I \frac{\sum_{j=0}^{N} \overline{\eta}^j G_1(2^j r)}{\sum_{j=0}^{N} \overline{\eta}^j 2^j} \tag{43}$$

where summation over k gives 2^j terms, as the statistics of the coefficients α do not depend on the position index k.

For large N, the following relation holds between scales r and $2r$:

$$S_1(2r) = I \frac{\sum_{j=0}^{N} \overline{\eta}^j G_1(2^{j+1} r)}{\sum_{j=0}^{N} \overline{\eta}^j 2^j} = 2I \frac{\sum_{j=0}^{N} \overline{\eta}^{j+1} G_1(2^{j+1} r)}{\sum_{j=0}^{N} \overline{\eta}^{j+1} 2^{j+1}} = 2S_1(r) \tag{44}$$

This implies, as expected, that $S_1(r) \sim r$, that is equation (40) where:

$$\zeta(1) = \log_2 \left(\frac{S_1(2r)}{S_1(r)} \right) = 1 \tag{45}$$

Note that (45) is consistent with (5) that states a form of conservation of measures over different scales.

The scaling of structure functions for any moment q can be computed in a similar way. Substitution of signal (33) into (31), exchanging integral and summation symbols, yields:

$$S_q(r) = < \left[\sum_{j=0}^{N} \sum_{k=0}^{2^j - 1} \alpha_{j,k} \int_{\xi}^{\xi+r} \psi_{j,k}(x) dx \right]^q > \tag{46}$$

The cumulant function, namely the connected part $S_q^c(r)$ of the structure function $S_q(r)$, has the following expression:

$$S_q^c(r) = \sum_{j=0}^{N} \sum_{k=0}^{2^j - 1} \alpha_{j,k}^q < \left[\int_{\xi}^{\xi+r} \psi_{j,k}(x) dx \right]^q > \sim r^{\zeta^c(q)} \tag{47}$$

14

The integral in square brackets of equation (47) can be substituted using the integral functions F of equation (41). Moreover, introducing another distribution $G_q(r) = < [F(\xi + r) - F(\xi)]^q >$, the following relation can replace the spatial average in equation (47):

$$< \left[F(2^j\xi + 2^j r - k) - F(2^j\xi - k) \right]^q > = 2^{-j} G_q(2^j r) \tag{48}$$

After elimination of summation over index k, and substitution of equations (38) and (39), the cumulant functions $S_q^c(r)$ take the following expression:

$$S_q^c(r) = I^q \frac{\sum_{j=0}^N \overline{\eta^{qj}} G_q(2^j r)}{\left[\sum_{j=0}^N \overline{\eta}^j 2^j \right]^q} \tag{49}$$

and over a scale $2r$:

$$S_q^c(2r) = I^q \frac{\sum_{j=0}^N \overline{\eta^{qj+1}} G_q(2^{j+1} r)}{\left[\sum_{j=0}^N \overline{\eta}^{j+1} 2^{j+1} \right]^q} \frac{2^q \overline{\eta}^q}{\overline{\eta^q}} = S_q^c(r) \frac{2^q \overline{\eta}^q}{\overline{\eta^q}} \tag{50}$$

We can finally estimate the exponent $\zeta^c(q)$, which exhibits the anomalous scaling of the cumulant functions S_q^c, as a function of the moments of the generator:

$$\zeta^c(q) = \log_2 \left(\frac{S_q^c(2r)}{S_q^c(r)} \right) = q \left(1 + \log_2 \overline{\eta} \right) - \log_2 \overline{\eta^q} \tag{51}$$

It is possible to show that functions S_q^c give the leading contribution to structure functions $S_q(r)$. The second order structure function can be written as a summation of two terms (the first one is the connected part and the second one is proportional to the square of the first order function): $S_2(r) = A_2 r^{\zeta^c(2)} + B_2 r^{2\zeta(1)} \sim r^{\zeta(2)}$, where A_2 and B_2 are constants. Using convexity of $\zeta^c(q)$, the second term on the right-hand side can be neglected for $r << 1$: the behavior of the second order structure function is $S_2(r) \sim r^{\zeta^c(2)}$. Inductively it can be shown for any moment q that the scaling (32) holds with $\zeta(q) \equiv \zeta^c(q)$ for $r << 1$.

In Appendix A we generalize the model presented here for the construction of multifractal measures $\phi(x_1, \cdots, x_d)$ with $\overline{x} \in [0,1]^d$ embedded on d-dimensional spaces. For these measures we derive the theoretical expectation for exponents $\zeta(q)$ that characterize the scaling of structure functions S_q:

$$S_q(r) = < \left[\int_{\xi_1}^{\xi_1 + r} dx_1 \cdots \int_{\xi_d}^{\xi_d + r} dx_d \, \phi(x_1, \cdots, x_d) \right]^q > \sim r^{\zeta(q)} \tag{52}$$

where

$$\zeta(q) = q\left(d + \log_2 \overline{\eta}\right) - \log_2 \overline{\eta^q} \tag{53}$$

3.2 Using the log-Poisson generator

We have already noted in section 2 that the log-Poisson distribution is suitable to include generalized scaling. Here we want to highlight how GESS can be introduced in synthetic rainfall data as discussed in subsection 3.1.

First of all, following the notation used in the previous subsection, we can introduce the log-Poisson distribution (15) by assuming that the random multiplier $\eta_{j,k}$ satisfies:

$$\eta_{j,k} = A_{j,k}\beta^{y_{j,k}} \tag{54}$$

where $A_{j,k}$ and β are parameters, while $y_{j,k}$ is a Poisson distributed random variable (16) with expectation $C_{j,k}$.

In order to display generalized scaling in a synthetic rainfall field, we assume that $A_{j,k} = g_1(2^{-j})/g_1(2^{-(j+1)})$ and $\exp C_{j,k} = g_2(2^{-j})/g_2(2^{-(j+1)})$, where g_1 and g_2 are two smooth functions whose properties have already been discussed in section 2. We remark that the quantity 2^{-j} should be considered equivalent to the "scale" r_j.

The expected scaling of signal $\phi(x)$ or more generally of $\phi(x_1, \cdots, x_d)$ can be evaluated using equations (53) and (17):

$$\zeta(q) = qd + c\,\frac{q\left(\beta - 1\right) - \left(\beta^q - 1\right)}{\ln 2} \tag{55}$$

where the exponent $\zeta(q)$ depends only on parameter β and on parameter $c = C_{j,k}$ that may be scale dependent.

By using the above definitions for the scale dependent random multiplier, we achieve the construction of a scale covariant synthetic rainfall data. As discussed in section 2, the structure functions $S_q(r)$ may not show scaling in r. However, we can observe GESS introducing the dimensionless structure functions $R_{q,n}(r)$:

$$R_{q,n}(r) = \frac{S_q(r)}{[S_n(r)]^{\frac{q}{n}}} \sim r^{\xi_n(q)} \tag{56}$$

16

where $\xi_n(q) = \zeta(q) - \zeta(n)q/n$. Properties of GESS can be now recovered by:

$$R_{p,n}(r) \sim R_{q,n}(r)^{\chi_n(p,q)} \tag{57}$$

where the exponents χ_n depend only on the β parameter that can be assumed scale invariant:

$$\chi_n(p,q) = \frac{\xi_n(p)}{\xi_n(q)} = \frac{\frac{p}{n}\left(\beta^n - 1\right) - \left(\beta^p - 1\right)}{\frac{q}{n}\left(\beta^n - 1\right) - \left(\beta^q - 1\right)} \tag{58}$$

The discussion presented in this section can be generalized for all infinitively divisible distributions.

3.3   Examples of synthetic fields

Examples of application of the wavelet model for generation of multifractal synthetic fields in R and R^2 are presented. The log-Poisson distribution was assumed for the random multipliers. Our aim is to compare the anomalous exponents, as predicted by the theory described in previous sections and in Appendix A, against anomalous scaling behavior observed in numerical simulations.

3.3.1   One-dimensional generations

Using the model described in 3.1, we have generated 64 synthetic samples $\phi(x)$ for $x \in [0,1]$, each one truncated after the 23rd cascade level, that is $N = 23$. Parameters of log-Poisson distribution (54) were $A_{j,k} = 1$, $\beta = 0.4$ and $C_{j,k} = c = 0.5$. The Gaussian function (36), with $\mu = \frac{1}{2}$ and $\sigma = 0.15$, was the basis function $\Psi(x)$. Figure 3 shows an example of synthetic signals between the 64 samples, that, for graphical reasons, is represented with a 2^{-12} resolution: the integral from $x = 0$ to $x = 1$ was scaled to one before plotting.

Structure functions S_q for moments $q = 1, 2, \cdots, 10$ were estimated on each of the 64 sample signals using definition (31), where averages $< \cdots >$ where applied to disjoint intervals. The exponents $\zeta(q)$ in (32) were then obtained by linear regressions in the log-log plane of structure functions versus spatial scales. In Figure 4 are plotted with error bars the average and the standard deviation of exponents $\zeta(q)$

on the 64 sample generations; in the same Figure the continuous line represents the theoretical expectation based on equation (55) with $d = 1$.

This last Figure gives evidence of the good agreement between theoretical predictions of the anomalous scaling laws of signals and the statistical properties of samples generated using Monte Carlo simulations.

3.3.2 Two-dimensional generations

The generalization of the wavelet decomposition in multi-dimensional spaces derived in Appendix A was used to generate 64 synthetic samples $\phi(x, y)$ in the domain $(x, y) \in [0, 1]^2$. The generator of the multiplicative process of coefficients α was a log-Poisson distribution (54) with parameters $A_{j,k} = 1$, $\beta = 0.4$ and $c = 0.7$: with this choice of parameters, the expected scaling (55) for synthetic fields is very close to the scaling found in rainfall fields produced by numerical simulations with a meteorological model (this case is analyzed in section 5). The basis function $\Psi(x)$ was again a Gaussian function (36) with parameters $\mu = \frac{1}{2}$ and $\sigma = 0.15$.

Each of the 64 generations was truncated after the 10-th cascade level ($N = 10$). Figure 5 shows a typical section of a synthetic field at full resolution 1024×1024, while in Figure 6 is plotted a sample field at reduced resolution 128×128 (the reduction was made only for graphical reasons). Before plotting the figures, the signals were scaled to have unit integrals in the domain $(x, y) \in [0, 1]^2$.

Structure functions $S_q(r)$, defined by equation (52) where $d = 2$, were estimated for moments $q = 1, 2, \cdots, 10$. Exponents $\zeta(q)$ of equation (52) were then estimated using linear regressions of logarithms of structure functions versus logarithms of spatial scales. In Figure 7 are plotted with error bars the average and the standard deviation of exponent $\zeta(q)$ of the 64 sample generations, together with a continuous line that represents the theoretical expectation based on equation (55).

As for the one-dimensional case, the statistical properties of synthetic fields in R^2, generated using the wavelet model, are in optimal agreement with the analytical derivation.

18

4 Statistical properties of rainfall in time

4.1 Analysis of Genova time series: the "external scale"

We now turn our attention to observed rainfall data. In this subsection we want to discuss the statistical properties of precipitation in time and discuss possible applications of the model described in the previous section on generating synthetic rainfall. With this aim we have analyzed the multifractal behavior of a high resolution rain time series observed at the University of Genova, where a tipping-bucket rain-gauge is sited. The series has a resolution of one minute in time and 0.2 mm of equivalent rainfall depth. The measurements are available from 1988 to 1995, with some small periods of inactivity, for a total of 2607 rainy and not rainy days.

We first investigate the statistical properties of the time series recorded in Genova. Next we show that a log-Poisson model gives a good fit to the observed scaling exponents. In the next subsection we generate synthetic signals with similar behavior of the structure functions and compare the extreme events distribution against the observed ones.

We define the time structure functions $S_q(\tau)$ as:

$$S_q(\tau) = < \left[\int_{\xi}^{\xi+\tau} P(t)dt \right]^q > \sim \tau^{\zeta(q)} \tag{59}$$

where $< \cdots >$ is an average operator over all possible disjointed sample of integrals at scale τ of the rainfall signal $P(t)$.

The structure functions S_q of the first 10 natural moments q of the observed signal $P(t)$ were computed at different time scales and plotted logarithmically in Figure 8 for time scales τ varying from 2 minutes to 2^{14} minutes (about 11 days) in powers of 2. From the Figure it is apparent that in the time series of Genova rainfall a threshold is located around 2^{10} minutes ($\simeq 12 \div 20$ hours). These results clearly reveal the presence of "external scale" in the scaling properties of $S_q(r)$.

In order to explain the presence of this "external scale", let us note that many authors have pointed out the description of the spatial and temporal variability of rainfall within the synoptic scale in terms of hierarchical structures [Austin and Houze, 1972]: from little rainfall cells that are aggregated in clusters within small

19

mesoscale areas (SMSA), up to the large mesoscale areas (LMSA). Many attempts to classify rain rates, velocities of storms, and durations that characterize the different spatial scales of the hierarchical process can be found in the literature [Rodriguez-Iturbe, 1986; Rodriguez-Iturbe et al., 1984; Waymire et al., 1984]. See for example Figure 9 in which a typical fall storm of high intensity is described using geosynchronous satellite infrared images: the spatial dimension of precipitating clusters in the synoptic area is $L \approx 300$ km and the velocity of advection of these structures is $U \approx$ 15-30 km/h. The duration in a fixed system between the beginning and the end of whole event is about $L/U \approx$ 10-20 hours. The average duration of extreme storms is in accordance with the threshold found on structure functions, which characterize different statistical behavior of the signal in time under this cut, where the structure functions are determined by the rainfall pattern internal to the storm, and over this cut, where the interarrivals of storms control the process.

A very interesting result can be obtained by looking at the generalized extended self similarity (57), namely by looking at the self scaling properties of the dimensionless structure functions $R_q(\tau) = S_q(\tau) / [S_4(\tau)]^{q/4}$. In Figure 10, we plot in a log-log plane the dimensionless structure functions R_q of moment $q = 7$ versus those of moment $q = 3$. First of all, we remark that a scaling relation is observed for all ranges of available time scales τ. Indeed, a threshold scale is no longer present in Figure 10, which clearly shows that the rainfall field is a self-similar process at any scale, in the range from 2 to 2^{14} minutes, and reflects the property of generalized extended self similarity discussed in section 2. Recalling equations (57) and (58), this result seems to state that synthetic rainfall time series can be generated using a time scale invariant β parameter in the log-Poisson generator (54). With this interpretation the effect of the "external scale" in the scaling behavior of structure function S_q, observed in Figure 8, can be modeled only by different values of the scale dependent parameter c of the Poisson distribution, as explained in section 3.2.

The exponents $\zeta(q)$ of equation (59) were estimated by a least square best fit between the logarithms of structure functions S_q and logarithms of the time scales for the two ranges, storm inner scales and storm external scales. In Figure 11 the estimations of $\zeta(q)$ are plotted for small scales from 2 minutes to 17 hours

and for large scales from 17 hours to 11 days. In the same Figure the theoretical expectation for exponent $\zeta(q)$, based on equation (55), for a log-Poisson generator with parameters $\beta = 0.30$ $c = 0.37$ for small scales and $\beta = 0.30$ $c = 0.95$ for large scales are also displayed by a continuous line.

4.2 Anomalous scaling of synthetic rainfall time series and extreme events distributions.

We now discuss the capability of the one-dimensional wavelet decomposition model to reproduce the rainfall depth process in time. For this purpose, by using the procedure discussed in section 3, we have generated a number of synthetic time series rainfall data, each one characterized by the same statistical properties, length, and resolution of those observed in Genova during the 2607 days between 1988 and 1995. Each daily generation was truncated at the 16-th cascade level on a 24 hour domain, which corresponds to a time resolution of about 1.32 seconds. The integral of each daily signal was then rescaled in order to have the same amount of precipitation observed on the corresponding day, making it dimensional. The time series were then obtained by joining each daily independent dimensional wavelet decomposition into the final sequence of 2607 days. After that the time series was "dressed" by reducing the time resolution to 1 minute, as the original series, and filtering the synthetic signal with a fictitious tipping-bucket rain-gauge: in such a way the simulated rainfall depth process was discretized every 0.2 mm like the real world process.

The effect of the "external threshold" was also investigated: two procedures in fact were used. In procedure I1, the threshold was supposed to be at 12 hours: the log-Poisson generator with parameters $\beta = 0.30$ and $c = 0.95$ was used on the first cascade level, and a second one with parameters $\beta = 0.30$ and $c = 0.37$ was used on the other 15 cascade levels. In procedure I2 the threshold was supposed to be at 24 hours and so a unique log-Poisson generator with constant parameters $\beta = 0.30$ and $c = 0.37$ was used on all the cascade levels.

A set of 30 synthetic time series was produced by using procedure I1 and a second set of the same size was produced for I2. In Figure 12 a sample of two realizations

21

of synthetic precipitation are compared with the observed one on the same day. The direct verification of the model was performed by estimating, from each series, the exponents $\zeta(q)$ with a least square best fit between the logarithms of sample structure functions and the logarithms of time scales. In Figure 13 the exponents $\zeta(q)$ estimated from the observed signal are compared with the mean and standard deviation of $\zeta(q)$ estimated from the sets of 30 series generated with procedure I2. Results with hypothesis I1 were very similar. Figure 13 give evidence of the capability of our model to reproduce the observed statistical properties of rainfall time series.

A quite interesting indirect validation was made by comparing the extreme values of the original series with those obtained by the synthetic ones. In particular, we have compared the parameters of the following distribution for the maximum rainfall height h accumulated during d hours that can be reached or exceeded every T years: $h = a(T)d^n$. To estimate the parameters n and $a(T)$ of this equation we have made the hypothesis that the yearly maxima height of rain precipitation in d hours follow a probability distribution of Gumbel type (EV1, Extreme Value Type 1). The parameters were estimated with the moments method using yearly maximum rainfall on 5 min, 10 min, 15 min, 30 min, 1 hour, 3 hours, 6 hours, and 12 hours. Results of this analysis can be found in Table 1 where we compare the estimates of parameters in the three cases: the observed time series and the 30 synthetic time series generated each according to hypothesis I1 or I2.

Even though the period of the recorded time series in Genova might be relatively short to capture the significant multifractal behavior of rainfall in time (i.e. parameter estimations can be probably reviewed), results on extreme event distributions are worthy of consideration for potential application of this model to estimation of extreme event distributions from coarse data.

5 Statistical properties of rainfall in space

We now turn our attention to the multifractal behavior of rainfall spatial fields. In particular, we have studied statistical properties of two kinds of spatial estimations

of rain: the first ones based on the radar measurements obtained during the GATE campaign; the second ones as output of a high resolution numerical simulation, performed with a meteorological limited area model (LAM) [Buzzi et al., 1994; Marrocu et al., in press].

The GATE spatial fields of precipitation were collected in the eastern Atlantic coast of Africa during two different periods in 1974: GATE1, the data-set of frames collected during the first period from 28 June to 15 July; and GATE2, the data-set of the second period from 28 July to 15 August.

Each frame represents the average rain rate every 15 minutes: data-set GATE1 contains 1715 frames, while data-set GATE2 contains 1512 frames. Fields are available with a 4 km spatial resolution in a regular square lattice 100×100, but data are really provided only within a 200 km radius of the center of each image. In the present work we used only a 64×64 grid centered in each image, in such a way that the rain rate is defined over each grid-point.

The precipitation depth fields obtained by the LAM simulation were saved every 6 hours over a regular grid 256×256 with a spatial resolution of about 10 km covering Europe, starting on 0GMT of 19 February 1991 and ending on 18GMT of the 22nd of the same month. The model was used in hindcasting mode, with initial and boundary conditions interpolated by the analysis of the ECMWF (European Center for Medium-range Weather Forecast), available every 6 hours. The LAM used for these experiments is a primitive equation model, and, as usual in meteorological models in operative configurations, the adiabatic contributions are solved separately from the diabatic contributions. The adiabatic contributions are the equations of momentum conservation (with the hydrostatic assumption in the vertical direction), the continuity equation, a thermodynamic equation and an equation for the water conservation. The diabatic contributions are provided by special parameterizations for large scale precipitation, vertical convection in cumuli, dry adjustment, radiative exchanges, horizontal and vertical diffusion, planetary boundary layer, soil moisture, and thermal balances [Emanuel, 1991; Geleyn and Hollingsworth, 1979; Louis et al., 1982]. The horizontal discretization is on a staggered grid of type C in the Arakawa classification, while the vertical discretization is on constant sigma coordinates. The

adiabatic equations were solved using an explicit leap-frog scheme, with a 9 second time-step for numerical stability, while the more computationally expensive diabatic contributions were computed every 10 minutes. Figure 14 shows a precipitation field obtained as output of the LAM integration.

The analysis of rainfall in space have been performed by computing the (anomalous) scaling behavior of the the space structure functions of order q, defined as follows:

$$S_q(r) = < \left[\int_\xi^{\xi+r} dx \int_\theta^{\theta+r} dy P(x,y) \right]^q > \sim r^{\zeta(q)} \qquad (60)$$

where $< \cdots >$ is an average operator over all possible disjointed samples of integrals on square domains (x,y) of side r, with starting integration points (ξ,θ); $P(x,y)$ is the spatial field of precipitation depth on a fixed time period.

From the GATE experiments not only rain spatial fields at the original time resolution of 15 minutes were taken into account, but also those obtained by averaging rain rates over 30 minutes, 1 hour, 3, 6, 12, and 24 hours. Two criteria were applied to select the fields to be used in the analysis. The first criterion imposes that at least 10% of grid points have a non zero measure of precipitation: in such a way we discard the fields without measures and those that are less relevant for the analysis. The second criterion requires a minimum correlation coefficient, fixed at level 0.995, for the linear regression between the logarithms of structure functions $S_{10}(r)$, defined by equation (60), and the logarithms of spatial scales r from 4 to 64 km, regularly sampled in the logarithmic scale with integer powers of 2. This second criterion guarantees a minimum statistical significance on estimation of exponents $\zeta(q)$.

The number N of fields, selected from each one of the original GATE1 and GATE2 data-sets, applying the two criteria exposed above, can be found in Table 2 for each duration considered in the analysis. Results of spatial multifractal analysis on the selected fields are summarized in Table 3 where we compare the averages of the first 10 exponents $\zeta(q)$, estimated in the range of scales from 4 to 64 km. In Table 2 are also listed for each data-set the values of parameters β and c obtained by imposing the values of sample exponents $\zeta(3)$ and $\zeta(8)$ in equation (55).

24

In a similar way we have also selected from the LAM data-set 13 of the 15 available precipitation fields accumulated every 6 hours. For this selection we have applied the criteria of minimum correlation coefficient (>0.995) for the linear regression between the logarithms of structure functions $S_{10}(r)$ and the logarithms of spatial scales r ranging from 10 to 160 km, sampled with integer powers of 2. Sample averages and standard deviations of the first 10 exponents $\zeta(q)$ based on 6-hour precipitation fields are plotted with error bars in Figure 15; in Table 3 the averages of multifractal exponents used to plot the Figure are compared with those obtained from the GATE data-sets. The Figure shows also that that the expected scaling (55) for the two-dimensional model with log-Poisson parameters $\beta = 0.4$ and $c = 0.7$ (the same as used for R^2 simulations discussed in subsection 3.3.2) is very close to the scaling found for LAM fields.

Results on spatial statistical properties of precipitation fields are also presented in Figure 16, where the sample averages of exponents $\zeta(q)$ estimated from LAM 6-hour rainfall fields are compared with exponents $\zeta(q)$ corresponding to the different accumulation times considered for GATE1 and GATE2 data-sets.

Although there are little differences between the $\zeta(q)$ estimated by the two GATE data-series, our analysis points out a strong dependence of the spatial statistical properties of the precipitation fields on the time duration, in which rainfall is accumulated. As expected, the multifractality of precipitation fields is more pronounced for short accumulation times. In other words, this means that for short times the behavior of precipitation fields is strongly intermittent and that the intermittency in space changes with duration.

Another very important result that comes from our work is the substantial coherence of the exponents $\zeta(q)$ determined for the 6-hour accumulated precipitation fields based on LAM simulations and those estimated from the GATE data-set at the same duration. Although the parameterization of rainfall processes in meteorological models are heavily simplified, the numerical simulation with the LAM has produced precipitation fields with statistical properties in good accordance with those observed in the GATE radar measurements.

6 Summary and concluding remarks

We outline and review the most relevant results of this work.

1) We have introduced the concept of scale covariance and extended self similarity as suitable generalizations of multifractal analysis. These concepts have been previously applied in the study of intermittency for three-dimensional flows. We argue that scale covariance and extended self similarity are useful concepts also in the framework of rainfall data.

2) We have shown how to compute synthetic rainfall fields which satisfy both anomalous scaling and extended self similarity. The method proposed in this paper is quite general and is not confined to the use of a particular probability distribution of the random multiplier. Moreover, the method was generalized in more than one dimension (in Appendix A) and to scale covariance fields.

3) Using time series of rainfall data, we have shown that the concept of scale covariance is indeed useful in explaining observed scaling properties of rainfall data. Our results also show that the log-Poisson distribution represents a good estimate for the anomalous scaling exponent.

4) We have compared observed time series against synthetic rainfall data, both having the same anomalous exponents and the same statistical samples. The comparison is quantitatively performed by looking at the statistical analysis of extreme events. The results we obtained allow us to argue that a multifractal description of rainfall data, in terms of scale covariance field, is an extremely good approximation to the observed statistical properties of rainfall time series.

5) We have shown that the rainfall field, as produced in meteorological models as limited area models, display anomalous scaling in rather good agreement with respect to the observed ones. Our analysis is somewhat limited by the small number of data sets examined. However, this result is worth mentioning since, although microphysical processes commonly applied in meteorological models are grossly parameterized, the LAM precipitation fields analyzed here preserve statistical properties observed in real rainfall. Another result that comes from the multifractal analysis on the GATE fields is that statistical behavior of precipitation in space is dependent

on the time duration over which rainfall is accumulated: as expected, precipitation fields display a stronger intermittency for shorter time durations.

In this paper we have used a rather simple log-Poisson model to fit observed anomalous exponents. We remark that other models may well achieve the same results; the log-Poisson distribution has been used both for its simplicity and for its physical meaning in the context of scale covariance fields (see section 2). Moreover, by using the log-Poisson distribution in our model to simulate random rainfall, the statistical properties of synthetic fields can be tuned with only two parameters. This represents a real advantage with respect to cluster-based models like the WGR model [Waymire et al., 1984], that require up to ten parameters to be estimated. In addition, the multifractal approach introduces relevant statistical constraints over a wide range of scales on the moments of signals. Further research on rainfall time series could investigate scale anomalies and the presence and localization of thresholds also at different sites, and the possible dependence of statistical properties and model parameters on geographical, orographic and climatic conditions.

Some open problems require further research and interactions in various areas and disciplines. A first open problem is strictly heuristic and concerns the physical interpretation of the multifractal behavior and intermittency observed in rainfall. Other problems are related to the use and application of precipitation fields from numerical weather prediction models as input to hydrological rainfall-runoff distributed models for forecasting flood events. It is well known that meteorological models supply forecasts on hundred or thousand square kilometer grid-size areas and hourly time scales. Rainfall-runoff models often require smaller resolution both in time and space, especially when applied to small basins. In this framework, a first issue to be resolved is how to link results discussed separately here on spatial and temporal statistical properties of rainfall, in order to apply the model directly for space-time downscaling of precipitation.

Appendix A   Construction of multidimensional fields

The one-dimensional model described in subsection 3.1 is here generalized for the construction of positive definite multifractal measures embedded in d-dimensional spaces. The construction of synthetic fields $\phi(x_1, \cdots, x_d)$ with $\overline{x} \in [0,1]^d$ is based on wavelet decomposition with coefficients extracted by a stochastic cascade:

$$\phi(x_1, \cdots, x_d) = \sum_{j=0}^{N} \sum_{k_1=0}^{2^j-1} \cdots \sum_{k_d=0}^{2^j-1} \alpha_{j,k_1\cdots k_d} \psi_{j,k_1\cdots k_d}(x_1, \cdots, x_d) \tag{A1}$$

where j is the cascade level index, varying from 0 (first element) to N (number of cascade levels); k_l is a position index on the x_l ($l = 1, \cdots, d$) axis, varying from 0 to $2^j - 1$ in the j-th cascade level; $\psi_{j,k_1\cdots k_d}(x_1, \cdots, x_d)$ is a wavelet on level j, characterized by the array of position indexes $(k_1, \cdots, k_d)$; while $\alpha_{j,k_1\cdots k_d}$ is the coefficient extracted from the stochastic cascade.

The wavelets ψ are now defined by a production of d one-dimensional basis wavelets $\Psi(x)$, positive definite and integrable for $x \in [0,1]$ and zero elsewhere:

$$\psi_{j,k_1\cdots k_d}(x_1, \cdots, x_d) = \prod_{l=1}^{d} 2^j \Psi(2^j x_l - k_l) \tag{A2}$$

The normalization in modulus of the basis function Ψ assures the normalization of each wavelet ψ, defined by the above equation.

The random cascade is constructed using a multiplicative process; the random generator η maps now each *father* term at $j-1$ level into 2^d new coefficients at level j:

$$\alpha_{j,k_1\cdots k_d} = \alpha_{j-1,\frac{k_1}{2}\cdots\frac{k_d}{2}}\eta \tag{A3}$$

Ensemble averages of q-moments of random variables α can be related to the statistics of the generator:

$$\overline{\alpha_{j,k_1\cdots k_d}^q} = \overline{\alpha_j^q} = \alpha_0^q \overline{\eta^q}^j \tag{A4}$$

Letting $I = \int_0^1 dx_1 \cdots \int_0^1 dx_d \phi(x_1, \cdots, x_d)$ be the integral of the synthetic signal, the first term of the random process must be:

$$\alpha_0 = \frac{I}{\sum_{j=0}^{N} 2^{jd} \overline{\eta}^j} \tag{A5}$$

In the following we show the scaling of signals (A1) and derive a theoretical prediction of the exponents $\zeta(q)$, that characterize structure functions $S_q(r)$:

$$S_q(r) = < \left[\int_{\xi_1}^{\xi_1+r} dx_1 \cdots \int_{\xi_d}^{\xi_d+r} dx_d \, \phi(x_1, \cdots, x_d) \right]^q > \sim r^{\zeta(q)} \tag{A6}$$

where the spatial average $< \cdots >$ can be now defined as an integral over all axes starting points ξ_l, with $l = 1, \cdots, d$. Moreover, using the symbol $< \cdots >_{\xi_l}$ to designate the spatial average on a generic axis x_l, we can write the relation:

$$< f > = c^d \int d\xi_1 \cdots \int d\xi_d f = < \cdots < f >_{\xi_1} \cdots >_{\xi_d} \tag{A7}$$

Structure functions $S_q(r)$ defined by equation (A6) can be rewritten after substitution of equations (A1) and (A2) and some manipulations between operators:

$$S_q(r) = < \left[\sum_{j=0}^{N} \sum_{k_1=0}^{2^j-1} \cdots \sum_{k_d=0}^{2^j-1} \alpha_{j,k_1 \cdots k_d} \prod_{l=1}^{d} 2^j \int_{\xi_l}^{\xi_l+r} \Psi(2^j x_l - k_l) dx_l \right]^q > \tag{A8}$$

Substituting equation (A7), the first order structure function has the following expression:

$$S_1(r) = \sum_{j=0}^{N} 2^{jd} \overline{\alpha_j} \prod_{l=1}^{d} < 2^j \int_{\xi_l}^{\xi_l+r} \Psi(2^j x_l - k_l) dx_l >_{\xi_l} \tag{A9}$$

Using equations (41), (42), (A4) and (A5), we can evaluate function S_1 at scale r:

$$S_1(r) = \sum_{j=0}^{N} 2^{jd} \overline{\alpha_j} \prod_{l=1}^{d} 2^{-j} G_1(2^j r) = \alpha_0 \sum_{j=0}^{N} \overline{\eta}^j \left[G_1(2^j r) \right]^d = I \frac{\sum_{j=0}^{N} \overline{\eta}^j \left[G_1(2^j r) \right]^d}{\sum_{j=0}^{N} \overline{\eta}^j 2^{jd}} \tag{A10}$$

and at scale $2r$:

$$S_1(2r) = I \frac{\sum_{j=0}^{N} \overline{\eta}^{j+1} \left[G_1(2^{j+1} r) \right]^d}{\sum_{j=0}^{N} \overline{\eta}^{j+1} 2^{(j+1)d}} 2^d = 2^d S_1(r) \tag{A11}$$

The exponent $\zeta(1)$ is equal to d:

$$\zeta(1) = \log_2 \left(\frac{S_1(2r)}{S_1(r)} \right) = d \tag{A12}$$

The connected part S_q^c of the q-th order structure function S_q defined by equation (A8) is the following:

$$S_q^c(r) = \sum_{j=0}^{N} 2^{jd} \overline{\alpha_j^q} \prod_{l=1}^{d} < \left[2^j \int_{\xi_l}^{\xi_l+r} \Psi(2^j x_l - k_l) dx_l \right]^q >_{\xi_l} \sim r^{\zeta^c(q)} \tag{A13}$$

Substituting equations (41) , (48), (A4) and (A5), we can write:

$$S_q^c(r) = \sum_{j=0}^{N} 2^{jd} \overline{\alpha_j^q} \prod_{l=1}^{d} 2^{-j} G_q(2^j r) = \alpha_0^q \sum_{j=0}^{N} \overline{\eta^{qj}} \left[G_q(2^j r) \right]^d = I^q \frac{\sum_{j=0}^{N} \overline{\eta^{qj}} \left[G_q(2^j r) \right]^d}{\left[\sum_{j=0}^{N} \overline{\eta^j} 2^{jd} \right]^q} \tag{A14}$$

and at scale $2r$:

$$S_q^c(2r) = I^q \frac{\sum_{j=0}^{N} \overline{\eta^{qj+1}} \left[G_q(2^{j+1} r) \right]^d}{\left[\sum_{j=0}^{N} \overline{\eta^{j+1}} 2^{(j+1)d} \right]^q} \frac{2^{qd} \overline{\eta^q}}{\overline{\eta^q}} = S_q^c(r) \frac{2^{qd} \overline{\eta^q}}{\overline{\eta^q}} \tag{A15}$$

Finally, we can estimate the scaling behavior of q-th order cumulant functions S_q^c as a function of the moments of the generator:

$$\zeta^c(q) = \log_2 \left(\frac{S_q^c(2r)}{S_q^c(r)} \right) = q \left(d + \log_2 \overline{\eta} \right) - \log_2 \overline{\eta^q} \tag{A16}$$

Also for multidimensional measures, it is possible to show, in an inductive way, that cumulant functions S_q^c give the leading contribution to structure functions $S_q(r)$ for any order q, that is:

$$S_q(r) \sim r^{\zeta(q)} \tag{A17}$$

where $\zeta(q) \equiv \zeta^c(q)$ for $r \ll 1$.

References

Austin, P. and Houze, R., Analysis of structure of precipitation patterns in New England., *J. Appl. Meteor.*, *11*, 926–935, 1972.

Benzi, R., Paladin, G., Parisi, G., and Vulpiani, A., On the multifractal nature of fully developed turbulence and chaotic systems, *J. Phys. A*, *17*, 3521–3531, 1984.

Benzi, R., Biferale, L., Crisanti, A., Paladin, G., Vergassola, M., and Vulpiani, A., A random process for the construction of multiaffine fields., *Physica D*, *65*, 352–358, 1993.

Benzi, R., Ciliberto, S., Tripiccione, R., Baudet, C., Massaioli, F., and Succi, S., Extended self-similarity in turbulent flows., *Phys. Rev. E*, *48*, R29–R32, 1993.

Benzi, R., Ciliberto, S., Baudet, C., and Chavarria, G., On the scaling of three-dimensional homogeneus and isotropic turbulence., *Physica D*, *80*, 385–398, 1995.

Benzi, R., Biferale, L., Ciliberto, S., Struglia, M. V., and Tripiccione, L., Generalized scaling in fully developed turbulence., *Physica D*, *96*, 162–181, 1996.

Buzzi, A., Fantini, M., Malguzzi, P., and Nerozzi, F., Validation of a limited area model in case of mediterranean cyclogenesis: surface fields and precipitation scores., *Meteorol. Atmos. Phys.*, *53*, 137–153, 1994.

Deidda, R., *Simulazione numerica delle proprietà statistiche dei campi di precipitazione*, Ph.D. thesis, University of Padua (Italy), 1997.

Emanuel, K., A scheme for representing cumulus convection in large-scale models, *J. Atmos.Sci.*, *48*(21), 2313–2335, 1991.

Frish, U., Sulem, P., and Nelkin, M., A simple dynamical model of fully developed turbulence., *J. Fluid Mech.*, *87*, 719–736, 1978.

Geleyn, J.-F. and Hollingsworth, A., An economical analytical methods for the computation of the interaction between scattered and line absorption of radiation., *Contrib. Atmos. Phys.*, *52*, 1–16, 1979.

Gupta, V. K. and Waymire, E. C., A statistical analysis of mesoscale rainfall as a random cascade., *J. Appl. Meteor.*, *32*, 251–267, 1993.

Hubert, P., Y.Tessier, Lovejoy, S., Schertzer, D., Schmitt, F., Ladoy, P., Carbonnel, J. P., Violette, S., and Desurosne, I., Multifractals and extreme rainfall events., *Geophys. Res. Lett.*, *20*(10), 931–934, 1993.

Kumar, P. and Foufoula-Georgiou, E., A multicomponent decomposition of spatial rainfall

fields. Part 1: Segregation of large- and small-scale feature using wavelet tranform. Part 2: Self-similarity in fluctuations., *Water Resour. Res.*, *29*(8), 2515–2532,2533–2544, 1993.

Ladoy, P., Schmitt, F., Schertzer, D., and Lovejoy, S., Variabilité multifractale des observations pluvimétriques à Nîmes, *C. R. Acad. Sci. Paris*, *317*, 775–782, 1993.

LeCam, L., A stochastic description of precipitation., in *4th Berkeley Symposium on Mathematical Statistics and Probability. vol. 3.*, pp. 165–186, University of California, Berkeley, 1961.

Louis, J.-F., Tiedtke, M., and Geleyn, J.-F., A short history of the PBL parameterization at ECMWF., in *Proceedings from the ECMWF Workshop on Planetary Boundary Layer Parameterization (25-27 November 1981).*, pp. 59–79, 1982.

Lovejoy, S. and Schertzer, D., Multifractals and rain., in *New Uncertainty Concepts in Hydrology and Water Resouces.*, edited by Z. W. Kunzewicz, vol. 235, University Press, Cambridge, 1992.

Marrocu, M., Scardovelli, R., and Malguzzi, P., Parallelization and performance of a meteorological Limited Area Model, *Parallel Computing*, in press.

Over, T. M. and Gupta, V. K., Statistical analysis of mesoscale rainfall: dependence of a random cascade generator on large-scale forcing., *J. Appl. Meteor.*, *33*, 1526–1542, 1994.

Rodriguez-Iturbe, I., Scale of fluctuation of rainfall models., *Water Resour. Res.*, *22*(9), 15S–37S, 1986.

Rodriguez-Iturbe, I., Gupta, V. K., and Waymire, E., Scale consideration of modelling of temporal rainfall., *Water Resour. Res.*, *20*(11), 1611–1619, 1984.

Schertzer, D. and Lovejoy, S., Physical modeling and analysis of rain and clouds by anysotropic scaling of multiplicative processes, *J. Geophys. Res. D.*, *92*, 9693–9714, 1987.

Tissier, Y., Lovejoy, S., and Schertzer, D., Universal multifractals: theory and observations for rain and clouds, *J. Appl. Meteor.*, *32*(2), 223–250, 1993.

Waymire, E., Gupta, V. K., and Rodriguez-Iturbe, I., A spectral theory for rainfall intensity at the meso-β scale., *Water Resour. Res.*, *20*(10), 1453–1465, 1984.

Tables

Table 1. Comparisons of parameters of the yearly maximum rainfall depth distribution $h = a(T)d^n$ estimated from the rain time series observed in Genova and from synthetic series generated with procedures I1 (threshold at 12 hours) and I2 (threshold at 24 hours). Parameter $a(T)$ is millimeter of rainfall depth, d is the duration in hours, T is the return period in years.

	n	$a(T)$		
		$T{=}5$	$T{=}10$	$T{=}25$
Observed time series	0.51	69	82	99
Synthetic time series: procedure I1	0.54	63	80	100
Synthetic time series: procedure I2	0.54	58	74	94

Table 2. Number N of selected fields from GATE1 and GATE2 data-sets for the spatial multifractal analysis and estimates of the log-Poisson parameters β and c for generation of synthetic spatial fields of rainfall depth at different durations.

	GATE1			GATE2		
duration	N	β	c	N	β	c
15 min	436	.42	1.00	316	.38	1.00
30 min	215	.43	.92	154	.40	.92
1 hour	128	.44	.83	95	.41	.88
3 hours	70	.44	.73	52	.44	.81
6 hours	46	.48	.77	40	.46	.75
12 hours	25	.55	.78	26	.51	.77
24 hours	13	.62	.71	14	.56	.68

Table 3. Averages of exponents $\zeta(q)$ in equation (60), estimated from GATE1 (G1) and GATE2 (G2) data-sets in the range of spatial scales 4÷64 km for different durations. For a comparison, averages of the multifractal exponents estimated from the 6-hour precipitation fields of the LAM data-set are also reported.

durations		$\zeta(2)$	$\zeta(3)$	$\zeta(4)$	$\zeta(5)$	$\zeta(6)$	$\zeta(7)$	$\zeta(8)$	$\zeta(9)$	$\zeta(10)$
15 min	G1	3.48	4.82	6.06	7.26	8.42	9.57	10.72	11.85	12.98
	G2	3.41	4.68	5.86	6.99	8.10	9.19	10.27	11.35	12.42
30 min	G1	3.55	4.97	6.30	7.59	8.85	10.09	11.32	12.54	13.76
	G2	3.48	4.84	6.11	7.34	8.54	9.72	10.89	12.06	13.22
1 hour	G1	3.59	5.07	6.49	7.85	9.19	10.50	11.80	13.09	14.37
	G2	3.52	4.92	6.25	7.53	8.78	10.01	11.23	12.44	13.65
3 hours	G1	3.64	5.18	6.67	8.11	9.52	10.92	12.29	13.66	15.02
	G2	3.61	5.11	6.54	7.93	9.28	10.62	11.94	13.25	14.55
6 hours	G1	3.67	5.25	6.76	8.22	9.66	11.07	12.47	13.85	15.23
	G2	3.66	5.22	6.72	8.18	9.60	11.01	12.40	13.78	15.16
	LAM	3.62	5.19	6.69	8.15	9.57	10.98	12.37	13.74	15.11
12 hours	G1	3.76	5.43	7.04	8.60	10.13	11.63	13.12	14.60	16.07
	G2	3.71	5.32	6.86	8.36	9.82	11.26	12.69	14.11	15.52
24 hours	G1	3.84	5.62	7.34	9.02	10.67	12.30	13.91	15.52	17.12
	G2	3.80	5.52	7.19	8.82	10.42	11.99	13.55	15.09	16.62

Figure Captions

Fig. 1. Plot of a Gaussian basis function $\Psi(x)$, defined by equation (36) with $\sigma = 0.15$, and of some wavelets $\psi_{j,k}(x)$ on the first two levels $j = 1, 2$, obtained by stretching and shifting the same basis function $\Psi(x)$ according to equation (34). The integral of each wavelet is normalized to unity.

Fig. 2. Graphical representation of the dyadic cascade process for $\alpha_{j,k}$ coefficients, where j is the level index, and k is the position index of the corresponding wavelet.

Fig. 3. A typical example of synthetic signal $\phi(x)$ generated in $x \in [0, 1]$ with the one-dimensional model and log-Poisson generator with parameters $\beta = 0.4$ and $c = 0.5$. The expansion was truncated at the 23rd level, but for graphical representation the signal is shown at 2^{-12} resolution. The integral of the signal from 0 to 1 is equal to unity.
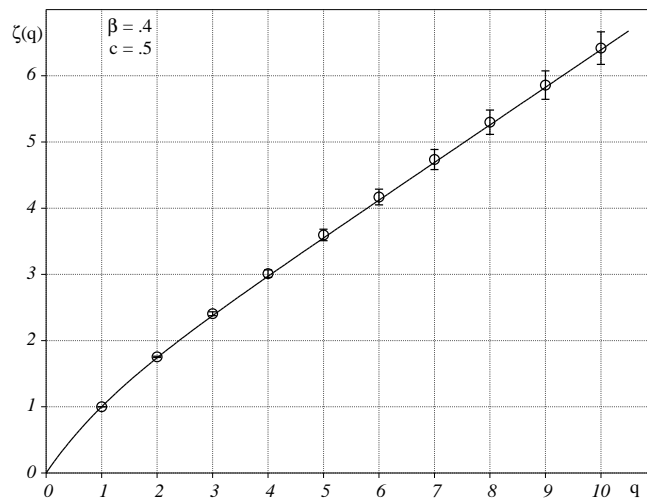
Fig. 4. The theoretical expectation (55) of moments $\zeta(q)$ for the one-dimensional ($d=1$) model with log-Poisson generator with parameters $\beta = 0.4$ and $c = 0.5$ (solid line). Error bars represent averages and standard deviations of $\zeta(q)$ estimated from the 64 synthetic signals.

Fig. 5. A typical section at 2^{-7} resolution, parallel to the x or y axis, of a two-dimensional synthetic field $\phi(x, y)$ selected between the 64 Monte Carlo simulations in R^2.
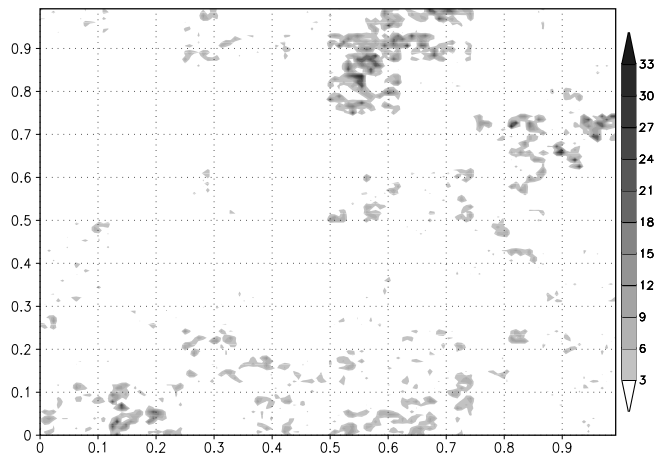
Fig. 6. A typical example of synthetic field $\phi(x, y)$ generated in $(x, y) \in [0, 1]^2$ with the two-dimensional model and the log-Poisson generator with parameters $\beta = 0.4$ and $c = 0.7$. The expansion was truncated at the 10th level, but for graphical representation the signal is shown at 2^{-7} resolution. The integral of the signal is equal to unity.

Fig. 7. The theoretical expectation (55) of moments $\zeta(q)$ for the two-dimensional ($d=2$) model with log-Poisson generator with parameters $\beta = 0.4$ and $c = 0.7$ (solid line). Error

bars represent averages and standard deviations of $\zeta(q)$ estimated from the 64 synthetic signals at 1024×1024 resolution.
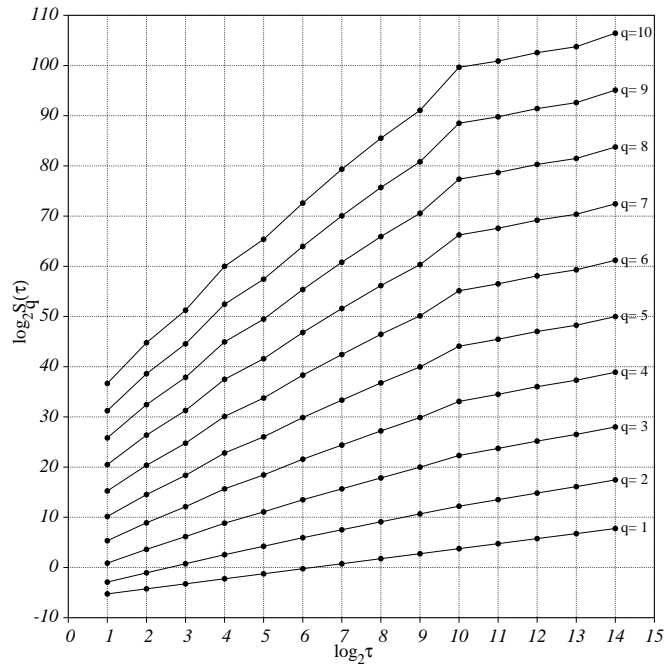
Fig. 8. The first 10 structure functions $S_q(\tau)$ of the rain time series observed at the University of Genova versus time scales τ in minutes. The range of time scales goes from 2 minutes to 2^{14} minutes (about 11 days). The "external scale" is marked by the threshold located around $\log_2 \tau = 10$ (about 17 hours).

Fig. 9. A geosynchronous satellite infrared image on the Mediterranean on 22 September 1992, 10 a.m. The area of high intensity rainfall travelling over the Gulf of Genova is highlighted by the circle with 300 km diameter.
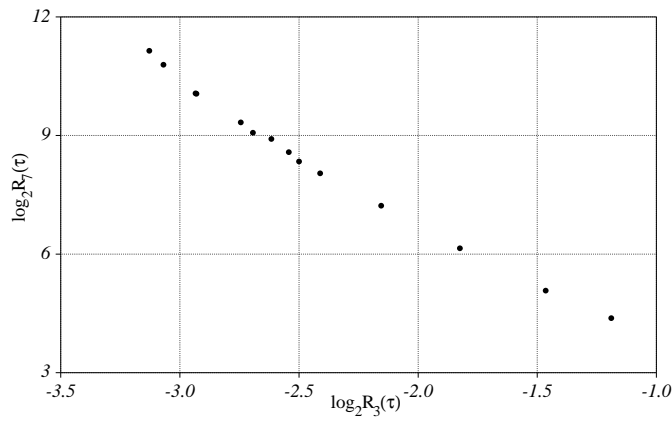
Fig. 10. Dimensionless structure functions $R_q(\tau)$ of moment $q = 7$ are plotted versus those of moment $q = 3$, with τ from 2 minutes to 2^{14} minutes. The threshold is no longer present, implying that the Genova rainfall time series satisfies generalized properties of extended self similarity.

**Fig. 11.** Anomalous scaling laws for small and large scales in the Genova rainfall time series. The estimates of exponents $\zeta(q)$ are marked with empty circles for small scales (2 minutes $\div$ 17 hours) and with filled circles for large scales (17 hours $\div$ 11 days). Continuous lines represent the corresponding expectations for the log-Poisson model with parameters $\beta = .30$, $c = 0.37$ (small scales), and $c = 0.95$ (large scales) based on equation (55).

Fig. 12. Millimeters of rainfall depth every 10 minutes on 14 January 1988 observed at the University of Genova (top) and synthetic signals (middle and bottom) characterized by the same daily total amount of precipitation (81.6 mm).

Fig. 13. Comparisons between the exponents $\zeta(q)$ of the observed Genova time series (filled circles) and averages and standard deviations (error bars) of those estimated by the synthetic set I2.

Fig. 14. A field of 6-hour precipitation depth (millimeters) over Europe produced by a limited area model integration. Spatial resolution is about 10 km, the grid is 256×256.

Fig. 15. Anomalous scaling laws of the 13 LAM precipitation fields selected for the spatial analysis. Averages and standard deviations of exponents $\zeta(q)$ are marked with error bars. The solid line is the expected scaling (55) for the two-dimensional model with log-Poisson parameters $\beta = 0.4$ and $c = 0.7$ (the same as used for R^2 simulations discussed in subsection 3.3.2).

Fig. 16. Averages of exponents $\zeta(q)$ of GATE1 and GATE2 data-sets for different durations from 15 minutes to 24 hours are compared. Note that the averages of $\zeta(q)$ estimated from LAM 6-hour precipitation fields (drawn with circles) are very close to the 6-hour GATE exponents.

Figures

Fig. 1. Plot of a Gaussian basis function $\Psi(x)$, defined by equation (36) with $\sigma = 0.15$, and of some wavelets $\psi_{j,k}(x)$ on the first two levels $j = 1, 2$, obtained by stretching and shifting the same basis function $\Psi(x)$ according to equation (34). The integral of each wavelet is normalized to unity.

Fig. 2. Graphical representation of the dyadic cascade process for $\alpha_{j,k}$ coefficients, where j is the level index, and k is the position index of the corresponding wavelet.

38

Fig. 3. A typical example of synthetic signal $\phi(x)$ generated in $x \in [0, 1]$ with the one-dimensional model and log-Poisson generator with parameters $\beta = 0.4$ and $c = 0.5$. The expansion was truncated at the 23rd level, but for graphical representation the signal is shown at 2^{-12} resolution. The integral of the signal from 0 to 1 is equal to unity.
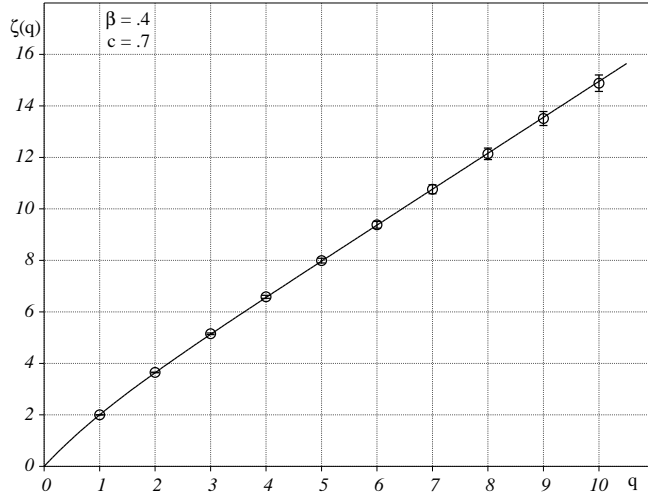

Fig. 4. The theoretical expectation (55) of moments $\zeta(q)$ for the one-dimensional (d=1) model with log-Poisson generator with parameters $\beta = 0.4$ and $c = 0.5$ (solid line). Error bars represent averages and standard deviations of $\zeta(q)$ estimated from the 64 synthetic signals.

39

Fig. 5. A typical section at 2^{-7} resolution, parallel to the x or y axis, of a two-dimensional synthetic field $\phi(x, y)$ selected between the 64 Monte Carlo simulations in R^2.

Fig. 6. A typical example of synthetic field $\phi(x, y)$ generated in $(x, y) \in [0, 1]^2$ with the two-dimensional model and the log-Poisson generator with parameters $\beta = 0.4$ and $c = 0.7$. The expansion was truncated at the 10th level, but for graphical representation the signal is shown at 2^{-7} resolution. The integral of the signal is equal to unity.

40

Fig. 7. The theoretical expectation (55) of moments $\zeta(q)$ for the two-dimensional ($d=2$) model with log-Poisson generator with parameters $\beta = 0.4$ and $c = 0.7$ (solid line). Error bars represent averages and standard deviations of $\zeta(q)$ estimated from the 64 synthetic signals at 1024×1024 resolution.

Fig. 8. The first 10 structure functions $S_q(\tau)$ of the rain time series observed at the University of Genova versus time scales τ in minutes. The range of time scales goes from 2 minutes to 2^{14} minutes (about 11 days). The "external scale" is marked by the threshold located around $\log_2 \tau = 10$ (about 17 hours).

41

Fig. 9. A geosynchronous satellite infrared image on the Mediterranean on 22 September 1992, 10 a.m. The area of high intensity rainfall travelling over the Gulf of Genova is highlighted by the circle with 300 km diameter.

Fig. 10. Dimensionless structure functions $R_q(\tau)$ of moment $q = 7$ are plotted versus those of moment $q = 3$, with τ from 2 minutes to 2^{14} minutes. The threshold is no longer present, implying that the Genova rainfall time series satisfies generalized properties of extended self similarity.

42

Fig. 11. Anomalous scaling laws for small and large scales in the Genova rainfall time series. The estimates of exponents $\zeta(q)$ are marked with empty circles for small scales (2 minutes $\div$ 17 hours) and with filled circles for large scales (17 hours $\div$ 11 days). Continuous lines represent the corresponding expectations for the log-Poisson model with parameters $\beta = .30$, $c = 0.37$ (small scales), and $c = 0.95$ (large scales) based on equation (55).
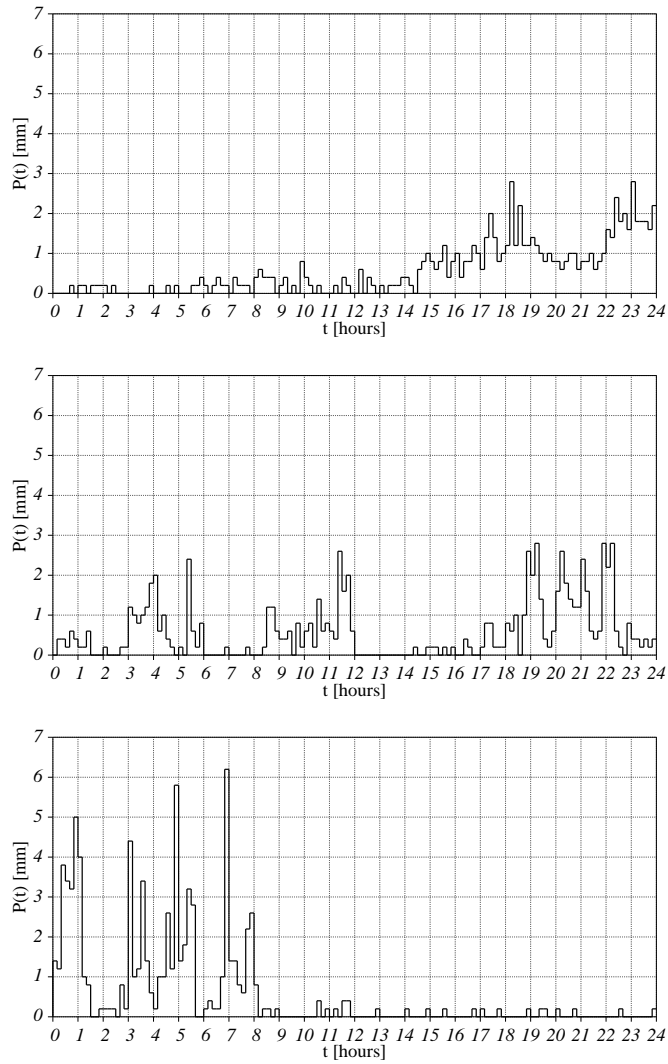
Fig. 12. Millimeters of rainfall depth every 10 minutes on 14 January 1988 observed at the University of Genova (top) and synthetic signals (middle and bottom) characterized by the same daily total amount of precipitation (81.6 mm).
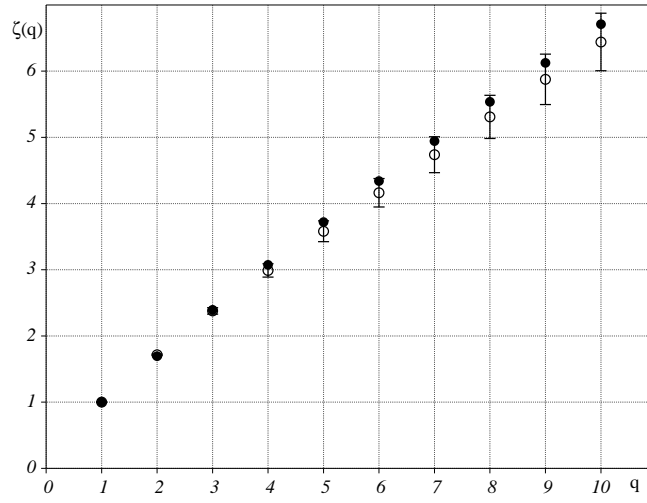
Fig. 13. Comparisons between the exponents $\zeta(q)$ of the observed Genova time series (filled circles) and averages and standard deviations (error bars) of those estimated by the synthetic set I2.
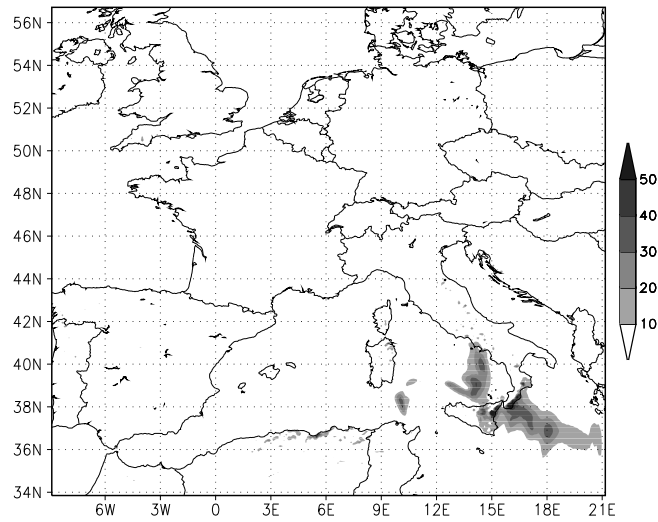

Fig. 14. A field of 6-hour precipitation depth (millimeters) over Europe produced by a limited area model integration. Spatial resolution is about 10 km, the grid is 256×256.
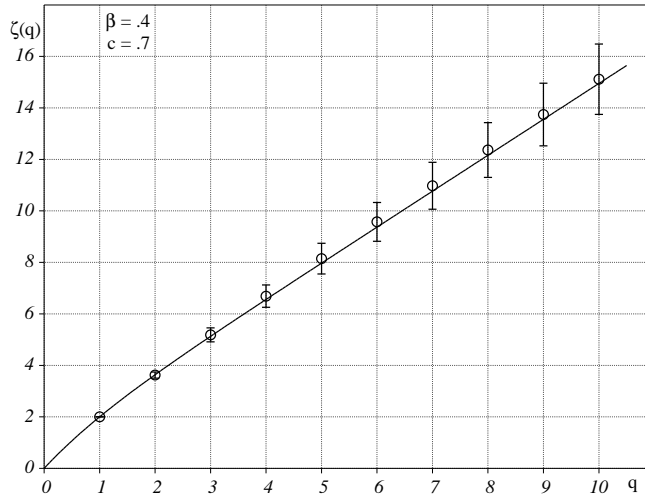
Fig. 15. Anomalous scaling laws of the 13 LAM precipitation fields selected for the spatial analysis. Averages and standard deviations of exponents $\zeta(q)$ are marked with error bars. The solid line is the expected scaling (55) for the two-dimensional model with log-Poisson parameters $\beta = 0.4$ and $c = 0.7$ (the same as used for R^2 simulations discussed in subsection 3.3.2).
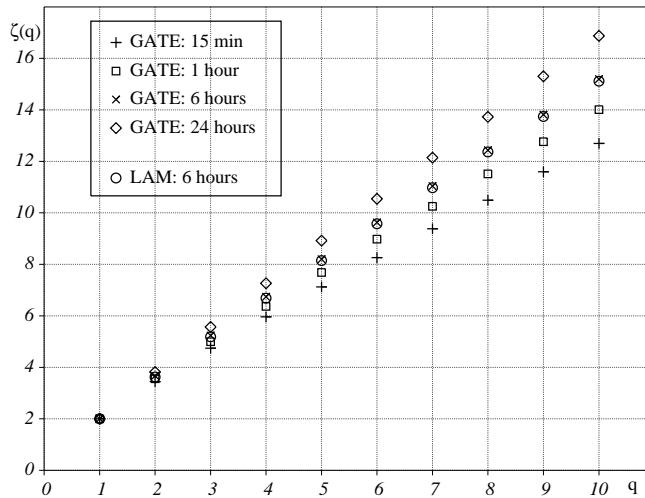

Fig. 16. Averages of exponents $\zeta(q)$ of GATE1 and GATE2 data-sets for different durations from 15 minutes to 24 hours are compared. Note that the averages of $\zeta(q)$ estimated from LAM 6-hour precipitation fields (drawn with circles) are very close to the 6-hour GATE exponents.

46